Clim. Past Discuss., 9, 2661–2680, 2013
www.clim-past-discuss.net/9/2661/2013/
doi:10.5194/cpd-9-2661-2013

Climate of the Past Discussions
Open Access

A high-resolution multi-proxy record of late Cenozoic environment change from central Taklimakan Desert, China

X. Wang, D. H. Sun, F. Wang, B. F. Li, S. Wu, F. Guo, Z. J. Li, Y. B. Zhang, and F. H. Chen

Key Laboratory of Western China's Environmental Systems (Ministry of Education), Lanzhou University, Lanzhou, 730000, China

Received: 6 May 2013 – Accepted: 15 May 2013 – Published: 24 May 2013

Correspondence to: D. H. Sun (dhsun@lzu.edu.cn)

Published by Copernicus Publications on behalf of the European Geosciences Union.

Abstract

The Taklimakan Desert in the Tarim Basin is the largest desert in Central Asia, and is regarded as one of the main dust sources to the Northern Hemisphere. Late Cenozoic sedimentary sequences with intercalated in-situ aeolian dune sands in this area preserve direct evidence for the Asian desertification. Herein, we report a high-resolution multi-proxy climatic record from the precise magnetostratigraphic dated Hongbaishan section in the central Taklimakan Desert. Our results show that a fundamental climate change, characterized by significant cooling, enhanced aridity, and intensified atmospheric circulation, occurred at 2.8 Ma. Good correlations between climate records in the dust sources and downwind areas suggest a broadly consistent climate evolution of northwestern China during the late Cenozoic, which is probably driven by the uplift of the Tibet Plateau and the Northern Hemisphere glaciation.

1 Introduction

The progressive retreat of the Tethys Sea and the stepwise uplift of the Tibetan Plateau during the Cenozoic resulted in the aridification and desertification in the Asian interior (e.g. Ramstein et al., 1997; Zhang et al., 2007; Manabe and Broccoli, 1990; Kutzbach et al., 1993; An et al., 2001; Molnar et al., 2010). These events led to the formation of large deserts in northwestern China and the accumulation of aeolian deposits in the downwind areas of the Chinese Loess Plateau (CLP) as far as the North Pacific (NP) (e.g. Liu, 1985; Rea et al., 1985).

Through study of sedimentary sections from the eastern CLP and NP, it is apparent that the desertification in the Asian interior initiated at 7–8 Ma (e.g. Sun et al., 1998; Ding et al., 1999; An et al., 2001), and enhanced at 3.4, 2.8, 1.8, 1.2, and 0.6 Ma (e.g. Sun and An, 2005; Sun et al., 2008). The recent discovery of Miocene loess sequences from the western CLP and its western areas has extended the Chinese dust history back to 25–22 Ma (e.g. Guo et al., 2002; Sun et al., 2010; Qiang et al., 2011).

CPD
9, 2661–2680, 2013

However, the aeolian records from NP illustrate that aeolian deposits have existed across the entire Cenozoic, exhibiting a stepwise increases in the mass accumulation rate, and suggesting a progressively enhanced aridity in the source regions (e.g. Rea et al., 1985, 1998). To obtain more direct evidence for the Asian aridification and desertification, a better knowledge of sedimentary records from source regions is required.

The Taklimakan Desert, with an area of 337 000 km^2, is the largest and oldest desert in Central Asia (Zhu et al., 1980), and is regarded as one of the main dust sources of the Northern Hemisphere (e.g. Washington et al., 2003; Zhang et al., 2003; Chen and Li, 2011). In the central Taklimakan Desert, continuous late Cenozoic sequences with intercalated in-situ aeolian dune sands preserve direct evidence for the Asian desertification. In this work, we report the multi-proxy indices of the Hongbaishan Section (hereafter refer to HBS Section), namely mean size, ultrafine component proportion, color reflectance, magnetic susceptibility, and frequency-depended magnetic susceptibility, based on the chronological frame established by paleomagnetic and ESR dating of two parallel sections (i.e. HBS and Mazhatagh Section) (Sun et al., 2011a). We attempt to provide the unique high-resolution multi-proxy climatic records for the dust source region during 4.2 to 0.99 Ma.

2 Geological setting and methods

The Tarim Basin is one of the largest closed basins in the word, bounded by Tibet to the south, the Pamir mountains to the west, and the Tien Shan mountains to the north. The basin is characterized by high mountains and alluvial fans at its periphery, and expansive flat sand sea (the Taklimakan Desert) in the central regions. Nevertheless, $\sim$ 240 km east-west ward mountains were developed in the central Taklimakan Desert in response to the India–Asia collision, from where Cenozoic sedimentary sequences cropped out (Fig. 1a).

Lying in the rain shadow of the Tibet Plateau, the climate in the Tarim Basin is extremely dry. The mean annual precipitation is less than 50 mm, whereas the mean

CPD
9, 2661–2680, 2013

annul evaporation is more than 2000 mm (Zhu et al., 1980), making it one of the driest desert on earth. Dominated by the westerlies, the region prevails northeasterly wind, which generate frequent storms at most times of the year (Aoki et al., 2005).

The HBS section (38°33′33″ N, 80°43′35″ E) is located at the eastern segment of the Mazatagh Mountain (Fig. 1a). The stratigraphic sequence is composed of Paleogene marine deposits and Neogene continental sediments (Fig. 1b), which are separated by a significant sedimentary hiatus (Yong et al., 1983). In this study, we focus on the continental succession, which is subdivided into 3 units (Fig. 2) according to the lithology, sedimentary facies, and proxy indices. Unit 1 (0–216 m interval), disconformably overlying the Paleocene marine strata, is about 219 m thick, mainly contains interbedding of reddish siltstone and red mudstone; occasionally, it contains reddish fine sandstone layers (Fig. 2a). Reddish siltstone and fine sandstone in this unit are characterized by thick parallel beddings in structure, and their grain-size distribution is mainly composed of a well-sorted coarse saltation component (ca > 250 μm), a poorly-sorted fine suspension component (ca 30–40 μm), and a small portion of ultrafine component (ca < 2 μm), suggesting a fluvial facies (e.g. Boggs, 1995; Reading, 1996; Sun et al., 2002). The commonly appearance of short suspension dust component or/and long suspension dust component (Fig. 2a) likely reflect strong wind reworking of the fluvial sediments under dry climate condition (e.g. Bullard and Livingstone, 2002). The deep-red mudstone in this unit is characterized by thin horizontal bedding and its grain-size distribution is mainly consists of a suspension components (ca 8–9 μm) and a small portion of ultrafine component (ca < 2 μm) (Fig. 2b), suggesting a lacustrine facies (e.g. Picard and High, 1981; Xiao et al., 2012). Unit 2 (216–304 m interval) comprises about 84-m-thick alternation of reddish-orange fine-grained sandstone, reddish siltstone, and deep-red laminated mudstone (Fig. 2b). The reddish-orange fine-grained sandstone is well sorted with large scale cross-beddings (Fig. 2c), and its grain-size distribution is characterized by a well-sorted aeolian saltation component (ca 50–250 μm) (Fig. 2c). These features fit well with typical aeolian dune sand (e.g. Pye and Tsoar, 2009; Reading, 1996). By contrast, reddish siltstone and deep-red laminated mudstone show similar

CPD
9, 2661–2680, 2013

sedimentary facies with Unit 1. Unit 3 (304–457 m interval), with a thickness of more than 155 m, is mostly grey-yellow aeolian dune sand and loess intercalated with fluvial sand and lacustrine clay (Fig. 2d). Loess generally has a tri-modal grain-size distribution that is composed of a short suspension dust component (ca 20–60 µm), a long suspension dust component (ca 10–15 µm), and a minor portion of ultrafine component (ca < 2 µm) (Fig. 2d); representing storm dust, background dust (Sun et al., 2004), and pedogenic clay (Sun et al., 2011b), respectively.

The HBS Section can be correlated with the Mazatagh Section (Sun et al., 2011a), KT1 Core (Zhang and Men, 2002), and KT2 Core (Xu et al., 2003) to the east (see section/drilling core locations in Fig. 1a), suggesting that the sedimentary record of the HBS Section reflects the broader paleo-environmental evolution of the central Tarim Basin.

Five hundred and thirty six samples were collected with an average sampling space of 0.85 m (~ 6 kyr) for analysis of proxy indices. The age of each sample was obtained by linear interpolation between the ages of geomagnetic polarity boundaries (e.g. Sun et al., 2011a). Grain size was measured on a Malvern Mastersizer 2000 laser grain-size analyzer, following the pre-treatment procedures of Konert and Vandenberghe (1997). Magnetic susceptibility were measured on a Bartington MS2 System with operating frequencies of 0.47 kHz (χ_{LF}) and 4.7 kHz (χ_{HF}), respectively. Frequency-depended magnetic susceptibility (χ_{FD}) was obtained by the formula: $\chi_{FD}(\%) = (\chi_{LF} - \chi_{HF})/\chi_{LF} \times 100$ (Dearing, 1994). For color measurement, samples were firstly dried at natural temperature, then were crushed without destructing grain size, and finally measured on a Konica-Minolta CM-700 color meter. All the measurements were performed in the Key Laboratory of Western China's Environmental systems, Lanzhou University.

CPD
9, 2661–2680, 2013

3 Results

3.1 Grain-size variation and its paleo-environmental implications

Grain size is closely linked to the processes and dynamics of transporting medium that carries grains, and thus, was frequently used in the paleo-envrionmental reconstructions as proxy for changes in property and potential energy of the transport medium (e.g. McCave, 1995; Porter, 2001; Ding et al., 2002; Duller et al., 2010). Mean size variations across the HBS Section are characterized by a pattern of high frequency fluctuations superimposed on an overall increasing trend (Fig. 3). The former one reflects the lithologic alternations between aeolian sand, loess, fluvial sand and lacustrine clay, and thus reveals the periodic environmental changes on orbital timescale. The later one represents a progressive enhancement of potential energy to the transporting medium from 4.2–0.99 Ma.

3.2 Variation in the ultrafine component proportion and its implication for the history of pedogenesis and chemical weathering

Grain-size data from the HBS Section reveal that an ultrafine component with a consistent modal size of ca 0.87 μm and a variable proportion of 0.3 to 10 % prevailed in the sequence (Fig. 2a–d). The ultrafine component proportion is high in the lacustrine and fluvial sediments (ca 5.99 %), and is low in the aeolian sand and loess (ca 2.76 %), showing linear correlations with soil moisture levels. Systematic work conducted on the loess-paleosol sequences from the CLP has shown that the ultrafine component proportion in the aeolian sediments is linked to pedogenic processes (Sun et al., 2011b). Alternatively, the ultrafine component proportion in the fluvial-lacustrine sediments is connected to the chemical weathering intensity (e.g. Chen et al., 2003; Lv et al., 2011; Wang et al., 2012a). As soil moisture and temperature are the main controlling factors in pedogenesis and chemical weathering (e.g. Chamley, 1989), it is clear that a lower proportion of the ultrafine components suggests a weaker soil development and a drier

CPD
9, 2661–2680, 2013

and colder climate, and vice versa. Therefore, the long-term variation in the ultrafine component proportion is interpreted as an indicator of pedogenesis and/or chemical weathering, which should reflect regional moisture conditions. At the HBS Section, the ultrafine component proportion increases gradually from 0–304 m (4.2–2.8 Ma), and subsequently decreases thereafter (2.8–0.9 Ma) (Fig. 3). The abrupt drop in the ultrafine component proportion at 304 m (2.8 Ma) reflects an enhanced aridity.

3.3 Color reflectance variation and its paleo-environmental implications

Color is the most visualized property of the sediments. A red color is ascribed to the presence of the mineral hematite (α-Fe_2O_3) that is formed in a hot and dry climate, while a yellow one is associated with goethite (α-FeOOH), which is associated with a colder and more humid climate (e.g. Reading, 1996; Viscarra Rossel et al., 2006). Therefore, variations between reds and yellows may reflect the change of oxidation state of the Fe iron that is mostly controlled by temperature (e.g. Barrón and Torrent, 1986; Thompson and Bell, 1996; Yang et al., 2001; Sun et al., 2011c). Lightness, by contrast, is mainly connected to the change of organic matter regime, which in turn reflects the climate change (e.g. Reading, 1996). A cooler and drier climate causes a slower decomposition rate of the organic matter and produces a lighter color (higher lightness) of the sediments, and vice visas. Therefore, lightness can serve as a proxy index of the decomposition rate of the organic matter that is mostly affected by the soil moisture and temperature. Throughout the HBS Section, redness (a^*) shows a gradual increasing trend from 0–304 m, and is followed by a decreasing trend thereafter, whereas, lightness (L) exhibits an overall negative relationship with the redness (Fig. 3). The dramatic decrease in redness and increase in lightness at 304 m (2.8 Ma) was interpreted as reflecting a significant climatic cooling and drying.

CPD
9, 2661–2680, 2013

3.4 Magnetic susceptibility variation and its implications for wind intensity

Magnetic susceptibility is a function of categories, concentration and particle size of the magnetic minerals (e.g. Dearing, 1994). At the HBS Section, magnetic susceptibility show distinctive values along with the lithologic alternations. Aeolian sand shows the lowest values (ca 5.6×10^{-8} SI), loess is slightly higher (ca 7.63×10^{-8} SI) but is lower than fluvial and lacustrine clay (ca 11.17×10^{-8} SI). These changes produce the high frequency fluctuations in the magnetic susceptibility curve (Fig. 3). By contrast, long-term variations of magnetic susceptibility in different sediments exhibit consistent increasing trends from bottom to top. For example, magnetic susceptibility of loess maintain the lowest value (ca 7.06×10^{-8} SI) in Unit 1, then it increases to higher values (ca 8.33×10^{-8} SI) in Unit 2, and finally reaches the highest values (ca 12.16×10^{-8} SI) in Unit 3. These features imply that unique forcing factors contribute to the long-term variations of magnetic susceptibility in different sediments. Rock magnetic analysis reveals that the appearance of polydomain magnetite in Unit 3 is response for the magnetic enhancement (Sun et al., 2011a), and the overall negative relationship between the magnetic susceptibility and frequency-depended magnetic susceptibility (a proxy for pedogenesis, see Sect. 3.5) (Fig. 3) also suggests a limited contribution of superparamagnetic ferrimagnets to the long-term variation of magnetic susceptibility. Since the wind intensity and/or the distance to the source regions are the main controlling factors affecting the concentration of the polymode ferrimagnets (Begét et al., 1989; Chlachula et al., 1998; Zan et al., 2011), and because of the late Cenozoic sediments in the central Tarim Basin are proximal deposits (Zhu et al., 1980; Si et al., 2009), it is apparent that a higher magnetic susceptibility indicates a stronger intensity of the atmospheric circulation, and vice versa. Across the HBS Section, magnetic susceptibility shows an overall increasing trend from bottom to top (Fig. 3), implying a stepwise strengthening of the atmospheric circulation. The dramatic increase in magnetic susceptibility at 304 m (2.8 Ma) reveals a significant intensified atmospheric circulation.

CPD
9, 2661–2680, 2013

3.5 Frequency-depended magnetic susceptibility variation and its paleo-environmental implications

Frequency-depended magnetic susceptibility reflects the concentration of viscous-superparamagnetic ferrimagnets that is mostly produced during the pedogenesis processes after deposited (e.g. Dearing et al., 1994; Evans and Heller, 2001). Since soil moisture and temperature are the major contributors in the pedogenic process (e.g. Chamley, 1989), it is obviously that a low frequency-depended magnetic susceptibility value equals a weaker soil equals a dried and colder climate, and vice versa (e.g. Evans and Heller, 2001). The variations of frequency-depended magnetic susceptibility in sequence thus are able to use as a proxy of pedogenisis. Across the HBS Section, the frequency-depended magnetic susceptibility increases gradually from 0–304 m interval, and subsequently decreases thereafter. The remarkable decrease in frequency-depended magnetic susceptibility at 304 m (2.8 Ma) yields an enhanced aridity.

4 Discussion and conclusion

From 4.2–3.4 Ma, the central Tarim Basin was a dry land, as indicated by the common occurrence of aeolian deposits and gypsum in the strata. Comparison of multi-proxy indices of the HBS Section with the Xifeng and Lingtai section from the eastern CLP (see section locations at Fig. 1a) suggests a warmer and drier climate in the Tarim Basin during this interval, owing to the HBS Section exhibit higher values of redness, and lower values of frequency-depended magnetic susceptibility and the ultrafine component proportion (Fig. 4). From 3.4 Ma onward, in-situ aeolian dune sands appeared and further developed in the sequence, suggesting the onset of the desertification in the central Tarim Basin initiated at this time. Nevertheless, the multi-proxy evidence presented here reveals a relatively warmer and more humid climate during 3.4–2.8 Ma, as redness, frequency-depended magnetic susceptibility and the ultrafine component proportion maintain the highest value in the sequence. In addition, the increases in

CPD
9, 2661–2680, 2013

magnetic susceptibility and sedimentation rate (Sun et al., 2011a) represent an intensified atmospheric circulation and increased sedimentary supply, respectively, which are essential for the dune buildings. The lithologic boundary at 2.8 Ma marks the first-order climate change in the central Tarim Basin. The change in sediment color from deep red to light yellow was interpreted as reflecting a significant climatic cooling and drying, the abrupt drop in frequency-depended magnetic susceptibility and the ultrafine component proportion indicate an enhanced aridity, while, the rise in mean size and magnetic susceptibility reflects an intensification of the wind intensity.

It has long been accepted that uplift of the Tibet Plateau played an important role in driving the Asian climate changes during the late Cenozoic (e.g. Manabe and Broccoli, 1990; Kutzbach et al., 1993; An et al., 2001; Molnar et al., 2010). Multi-proxy indices presented here provide independent sedimentary and climatic evidence for the previous understandings: (1) the appearance of the earliest in-situ aeolian dune sand, at 3.4 Ma, is associated with an increased sedimentation rate in the Tarim Basin (Sun et al., 2011a), and is correlated broadly with the accumulation of thick coarse-grained conglomerates in the north margin of the Kunlun Mountain, which was interpreted as a consequence of the uplift of the northern Tibet Plateau (e.g. Huang and Chen, 1980; Zheng et al., 2000); (2) the climate of the central Tarim Basin during 3.4 to 2.8 Ma was characterized by hot, relatively humid, and strengthened wind intensity, and corresponds to the simultaneous intensification of both summer and winter eastern Asian monsoons over the CLP (An et al., 2001). It is difficult to attribute to this climate change to the increase in the volume of continental ice sheets during this interval (Fig. 4), as such an event should produce a weakening of the summer monsoon and a strengthening of the winter monsoon in the Monsoon dominated area, as well as a cooling over the western China (Prell et al., 1992). The continued growth of the Tibet Plateau along its northern and eastern margins (e.g. An et al., 2001; Zheng et al., 2000) contributed to the regional climate changes.

The remarkable changes of multi-proxy indices from the central Tarim Basin at 2.8 Ma can be correlated with those from the CLP and the NP (Fig. 4, Sun et al.,

CPD
9, 2661–2680, 2013

2008, 2010; Wang et al., 2012b; Sun and An, 2005; Rea et al., 1998), which are consistent with the onset of the major Northern Hemisphere glaciation around 2.75 Ma (e.g. Ding et al., 1995; Lisiecki and Raymo, 2005), suggesting a causal relationship. Numerical modeling has illustrated that the expansion of the ice sheet would cause the southward shift of the polar front and the intensification of the Mongolia high and Siberia high system in North Asia, which in turn would result in a southward migration of Westerly and strengthening of the East Asian winter monsoon (Porter and An, 1995). The strengthened circulation intensity, together with the enhanced aridity in the source regions, resulted in the further desertification in the Asian interior.

Multi-proxy evidence from the HBS Section suggests a fundamental environmental change, characterized by significant cooling, enhanced aridity, and intensified atmospheric circulation, occurred at 2.8 Ma in the Tarim Basin. Good correlations between climate records from source region and downwind areas suggest a broadly consistent climate evolution over the northwestern Chian during the late Cenozoic. We attribute the desertification in the Tarim Basin to the uplift of the Tibet Plateau and to Northern Hemisphere glaciations.

Acknowledgements. Financial support for this research was provided by National Science Foundation of China grants (40625009), National Basic Research Program of China (2010CB833400), National Innovative Research Team Project (40121061), and the Fundamental Research Funds for the Central Universities (lzujbky-2013-118). The author thanks for Brian P. Kraatz for improve the English usage.

References

An, Z., Kutzbach, J., Prell, W., and Porter, S.: Evolution of Asian monsoons and phased uplift of the Himalaya–Tibetan plateau since Late Miocene times, Nature, 411, 62–66, 2001.

Aoki, I., Kurosaki, Y., Osada, R., Sato, T., and Kimura, F.: Dust storms generated by mesoscale cold fronts in the Tarim Basin, Northwest China, Geophys. Res. Lett., 32, L06807, doi:10.1029/2004GL021776, 2005.

CPD
9, 2661–2680, 2013

Barrón, V. and Torrent, J.: Origin of red–yellow mottling in a Ferric Acrisol of southern Spain, Z. Pflanz. Bodenkunde, 150, 308–313, 1987.
Begét, J. and Hawkins, D.: Influence of orbital parameters on Pleistocene loess deposition in central Alaska, Nature, 337, 151–153, 1989.
Boggs, S.: Principles of Sedimentology and Stratigraphy, Prentice Hall, Upper Saddle River, NJ, USA, 1995.
Bullard, J. and Livingstone, I.: Interactions between aeolian and fluvial systems in dryland environments, Area, 34, 8–16, 2002.
Chamley, H.: Clay Sedimentology, Springer-Verlag, New York, 1989.
Chen, J. and Li, G.: Geochemical studies on the source region of Asian dust, Sci. China Ser. D, 54, 1279–1301, 2011.
Chen, S., Wang, S., Jin, Z., and Shen, J.: Chemical weathering and environmental change records of the last 2.8 Ma in the Central Tibetan Plateau, Geol. J. China Univ., 9, 19–29, 2003.
Chlachula, J.: The Siberian loess record and its significance for reconstruction of Pleistocene climate change in north-central Asia, Quaternary Sci. Rev., 22, 1879–1906, 2003.
Dearing, J.: Environmental Magnetic Susceptibility, Chi Publ, Kenilworth, UK, 1994.
Ding, Z., Liu, T., Rutter, N., Yu, Z., Guo, Z., and Zhu, R.: Ice-volume forcing of East Asian winter monsoon variations in the past 800,000 years, Quaternary Res., 44, 149–159, 1995.
Ding, Z., Xiong, S., Sun, J., Yang, S., Gu, Z., and Liu, T.: Pedostratigraphy and paleomagnetism of a 7.0 Ma eolian loess-red clay sequence at Lingtai, Loess Plateau, north-central China and the implications for paleomonsoon evolution, Palaeogeogr. Palaeocl., 152, 49–66, 1999.
Ding, Z., Derbyshire, E., Yang, S., Yu, Z., Xiong, S., and Liu, T.: Stacked 2.6-Ma grain size record from the Chinese loess based on five sections and correlation with the deep-sea δ^{18}O record, Paleoceanography, 17, 1033, doi:10.1029/2001PA000725, 2002.
Duller, R., Whittaker, A., Fedele, J., Whitchurch, A., Springett, J., Smithells, R., Fordyce, S., and Allen, P.: From grain size to tectonics, J. Geophys. Res., 115, F03022, doi:10.1029/2009JF001495, 2010.
Evans, M. and Heller, F.: Magnetism of loess/palaeosol sequences: recent developments, Earth-Sci. Rev., 54, 129–144, 2001.
Guo, Z., Ruddiman, W., Hao, Q., Wu, H., Qiao, Y., Zhu, R., Peng, S., Wei, J., Yuan, B., and Liu, T.: Onset of Asian desertification by 22 Myr ago inferred from loess deposits in China, Nature, 416, 159–163, 2002.

CPD
9, 2661–2680, 2013

Huang, J. and Chen, B.: On the formation Of Pliocene–Quaternary molasses in the Tethys–Himalayan tectonic domain and its relation with the Indian plate motion, in: Scientific Papers on Geology for International Exchange, Prepared for the 26th International Geological Congress 1 Tectonic Geology and Geological Mechanics, Beijing, 1–14, 1980.

Konert, M. and Vandenberghe, J. E. F.: Comparison of laser grain size analysis with pipette and sieve analysis: a solution for the underestimation of the clay fraction, Sedimentology, 44, 523–535, 1997.

Kutzbach, J., Prell, W., and Ruddiman, W.: Sensitivity of Eurasian climate to surface uplift of the Tibetan Plateau, J. Geol., 101, 177–190, 1993.

Liu, T.: Loess and the Environment, China Ocean Press, Beijing, 251 pp., 1985.

Lv, Y., Zhao, J., Huang, W., Tao, S., and An, C.: Decomposition of the grain-size component and its climate implication from Lake Barkol, Xinjiang, Acta Sedimentol. Sin., 29, 134–142, 2011.

Manabe, S. and Broccoli, A.: Mountains and arid climates of middle latitudes, Science, 247, 192–195, 1990.

McCave, I., Manighetti, B., and Beveridge, N. A. S.: Circulation in the glacial North Atlantic inferred from grain-size measurements, Nature, 374, 149–152, 1995.

Molnar, P., Boos, W., and Battisti, D.: Orographic controls on climate and paleoclimate of Asia: thermal and mechanical roles for the Tibetan Plateau, Annu. Rev. Earth Pl. Sc., 38, 77–102, 2010.

Picard, M. D. and High, J.: Physical stratigraphy of ancient lacustrine deposits, in: Recognition of Ancient Sedimentary Environments, edited by: Rigby, J. K. and Hamblin, W. K., 16, Soc. Econ. Paleontol. Mineral., Spec. Publ., Tulsa, 108–145, 1981.

Porter, S.: Chinese loess record of monsoon climate during the last glacial-interglacial cycle, Earth-Sci. Rev., 54, 115–128, 2001.

Pye, K. and Tsoar, H.: Aeolian Sand and Sand Dunes, Springer, Berlin, 2009.

Qiang, X., An, Z., Song, Y., Chang, H., Sun, Y., Liu, W., Ao, H., Dong, J., Fu, C., Wu, F., Lu, F., Cai, Y., Zhou, W., Cao, J., Xu, X., and Ai, L.: New eolian red clay sequence on the western Chinese Loess Plateau linked to onset of Asian desertification about 25 Ma ago, Sci. China Ser. D, 54, 1–9, 2011.

Ramstein, G., Fluteau, F., Besse, J., and Joussaume, S.: Effect of orogeny, plate motion and land-sea distribution on Eurasian climate change over the past 30 million years, Nature, 386, 788–795, 1997.

CPD
9, 2661–2680, 2013

Rea, D., Leinen, M., and Janecek, T.: Geologic approach to the long-term history of atmospheric circulation, Science, 227, 721–725, 1985.
Rea, D., Snoeckx, H., and Joseph, L.: Late Cenozoic eolian deposition in the North Pacific: Asian drying, Tibetan uplift, and cooling of the Northern Hemisphere, Paleoceanography, 13, 215–224, 1998.
Reading, H.: Sedimentary Environments: Processes, Facies, and Stratigraphy, Wiley-Blackwell, Oxford, 1996.
Si, J., Li, H., Pei, J., and Pan, J.: Uplift of northwest margin of Tibetan Plateau: indicated by zircon LA ICP-MS U-Pb dating of conglomerate from Mazartagh, Tarim Basin, J. Earth Sci., 20, 401–416, 2009.
Sun, D., Shaw, J., An, Z., Cheng, M., and Yue, L.: Magnetostratigraphy and paleoclimatic interpretation of a continuous 7.2 Ma Late Cenozoic eolian sediments from the Chinese Loess Plateau, Geophys. Res. Lett., 25, 85–88, 1998.
Sun, D., Bloemendal, J., Rea, D., Vandenberghe, J., Jiang, F., An, Z., and Su, R.: Grain-size distribution function of polymodal sediments in hydraulic and aeolian environments, and numerical partitioning of the sedimentary components, Sediment. Geol., 152, 263–277, 2002.
Sun, D., Bloemendal, J., Rea, D., An, Z., Vandenberghe, J., Lu, H., Su, R., and Liu, T.: Bimodal grain-size distribution of chinese loess, and its palaeoclimatic implications, Catena, 55, 325–340, 2004.
Sun, D., Su, R., Bloemendal, J., and Lu, H.: Grain-size and accumulation rate records from Late Cenozoic aeolian sequences in northern China: implications for variations in the East Asian winter monsoon and westerly atmospheric circulation, Palaeogeogr. Palaeocl., 264, 39–53, 2008.
Sun, D., Bloemendal, J., Yi, Z., Zhu, Y., Wang, X., Zhang, Y., Li, Z., Wang, F., Han, F., and Zhang, Y.: Palaeomagnetic and palaeoenvironmental study of two parallel sections of late Cenozoic strata in the central Taklimakan Desert: implications for the desertification of the Tarim Basin, Palaeogeogr. Palaeocl., 300, 1–10, 2011a.
Sun, D., Su, R., Li, Z., and Lu, H.: The ultrafine component in Chinese loess and its variation over the past 7.6 Ma: implications for the history of pedogenesis, Sedimentology, 58, 916–985, 2011b.
Sun, J., Ye, J., Wu, W., Ni, X., Bi, S., Zhang, Z., Liu, W., and Meng, J.: Late Oligocene–Miocene mid-latitude aridification and wind patterns in the Asian interior, Geology, 38, 515–518, 2010.

CPD
9, 2661–2680, 2013

Sun, Y. and An, Z.: Late Pliocene–Pleistocene changes in mass accumulation rates of eolian deposits on the central Chinese Loess Plateau, J. Geophys. Res., 110, D23101, doi:10.1029/2005JD006064, 2005.
Sun, Y., An, Z., Clemens, S., Bloemendal, J., and Vandenberghe, J.: Seven million years of wind and precipitation variability on the Chinese Loess Plateau, Earth Planet. Sc. Lett., 297, 525–535, 2010.
Sun, Y., He, L., Liang, L., and An, Z.: Changing color of Chinese loess: geochemical constraint and paleoclimatic significance, J. Asian Earth Sci., 40, 1131–1138, 2011.
Thompson, J. and Bell, J.: Color index for identifying hydric conditions for seasonally saturated mollisols in Minnesota, Soil Sci. Soc. Am. J., 60, 1979–1988, 1996
Viscarra Rossel, R., Minasny, B., Roudier, P., and McBratney, A.: Colour space models for soil science, Geoderma, 133, 320–337, 2006.
Wang, F., Sun, D., Guo, F., Wang, X., Li, Z., Zhang, Y., Li, B., and Wu, S.: Quantitative reconstruction of paleo-temperature and paleo-precipitation of Lingtai profile in Loess Plateau during the past 7 Ma, J. Earth Environ., 3, 791–791, 2012b.
Wang, X., Sun, D., Wang, F., Li, B., and Wu, S.: The ultrafine component record from the late Cenozoic sequence in the central Tarim Basin and its palaeoclimatic implication, Mar. Geol. Quatern. Geol., 32, 143–151, 2012a.
Washington, R., Todd, M., Middleton, N., and Goudie, A.: Dust–storm source areas determined by the Total Ozone Monitoring Spectrometer and surface observations, Ann. Assoc. Am. Geogr., 93, 297–313, 2003.
Xiao, J., Chang, Z., Fan, J., Zhou, L., Zhai, D., Wen, R., and Qin, X.: The link between grain-size components and depositional processes in a modern clastic lake, Sedimentology, 59, 1050–1062, 2012.
Xu, J., Yang, Z., Zheng, H., Zhang, J., Lin, F., and Shi, Y.: Quaternary magnetic stratigraphy of the Tarim Basin, J. Stratigr., 27, 256–261, 2003.
Yang, S., Fang, X., Li, J., An, Z., Chen, S., and Hitoshi, F.: Transformation functions of soil color and climate, Sci. China Ser. D, 44, 218–226, 2001.
Yong, T., Shan, J., and Wang, S.: Several geological issues about the Marzartag – together with the geological age of the Taklamakan desert, Xinjiang Petrol. Geol., 4, 1–9, 1983.
Zan, J., Fang, X., Yang, S., Nie, J., and Li, X.: A rock magnetic study of loess from the West Kunlun Mountains, J. Geophys. Res., 115, B10101, doi:10.1029/2009JB007184, 2010.

CPD
9, 2661–2680, 2013

Zhang, H. and Men, G.: Stratigraphic subdivision and climatic change of the Quaternary of the center Taklimakan Deaert, Xinjiang Geol., 20, 256–261, 2002.
Zhang, X., Gong, S., Zhao, T., Arimoto, R., Wang, Y., and Zhou, Z.: Sources of Asian dust and role of climate change versus desertification in Asian dust emission, Geophys. Res. Lett., 30, 2272, doi:10.1029/2003GL018206, 2003.
Zhang, Z., Wang, H., Guo, Z., and Jiang, D.: What triggers the transition of palaeoenvironmental patterns in China, the Tibetan Plateau uplift or the Paratethys Sea retreat?, Palaeogeogr. Palaeocl., 245, 317–331, 2007.
Zheng, H., Powell, C., An, Z., Zhou, J., and Dong, G.: Pliocene uplift of the northern Tibetan Plateau, Geology, 28, 715–718, 2000.
Zhu, Z., Wu, Z., Liu, S., and Di, X: An Outline on Chinese Deserts, Science Press, Beijing, 107 pp., 1980.

CPD
9, 2661–2680, 2013

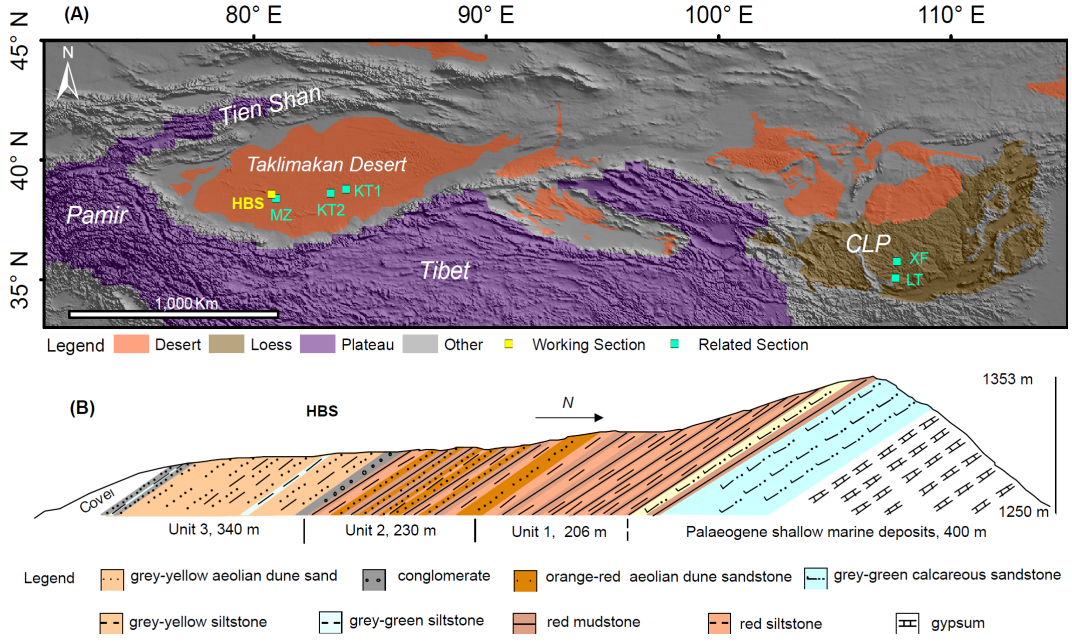

Fig. 1. Present geographic environment in northwestern China projected on the topographic images of a digital elevation model **(A)** and sketches geological map of the HBS Section **(B)**.

CPD
9, 2661–2680, 2013

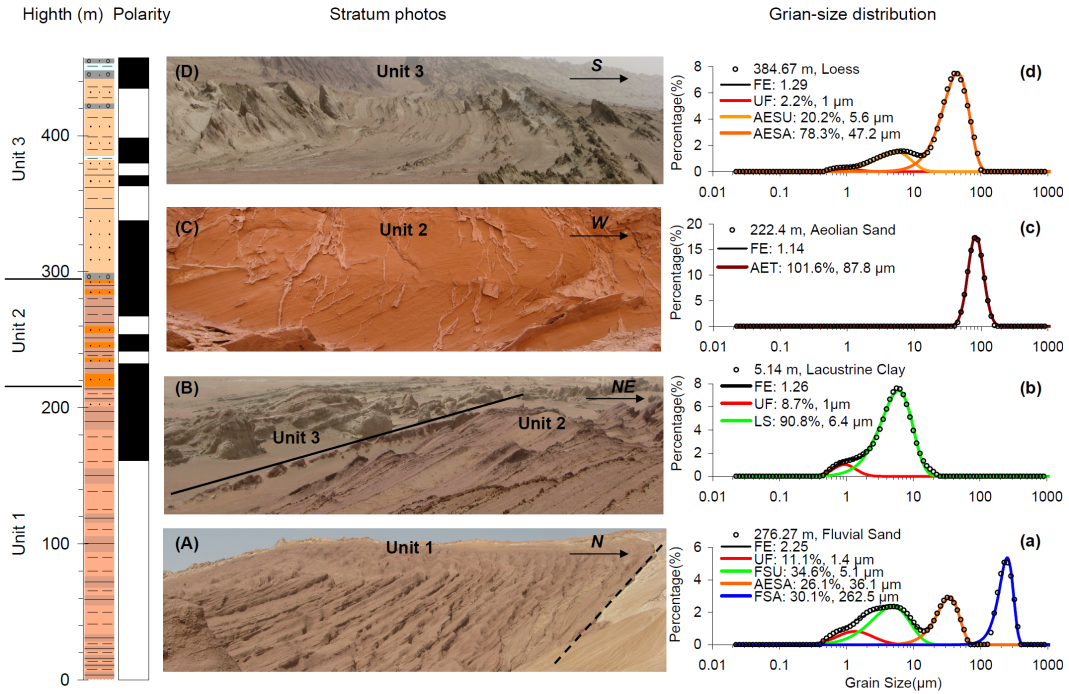

Fig. 2. Stratigraphy and magnetostratigraphy (Sun et al., 2011a) of the HBS Section. Stratum photos and grain-size distribution of representative samples are given to show the sedimentary facies across the section. The grain-size distribution of bulk samples was partitioned using the method of Sun et al. (2002). Abbreviations: FE – fitting curve with error, UF – ultrafine component, AESU – aeolian suspension component, AESA – aeolian saltation component, AET – aeolian traction component, LS – lacustrain suspension component, FSU – fluvial suspension component, FSA – fluvial saltation component. The lithology types of the strata are the same as in Fig. 1.

CPD
9, 2661–2680, 2013

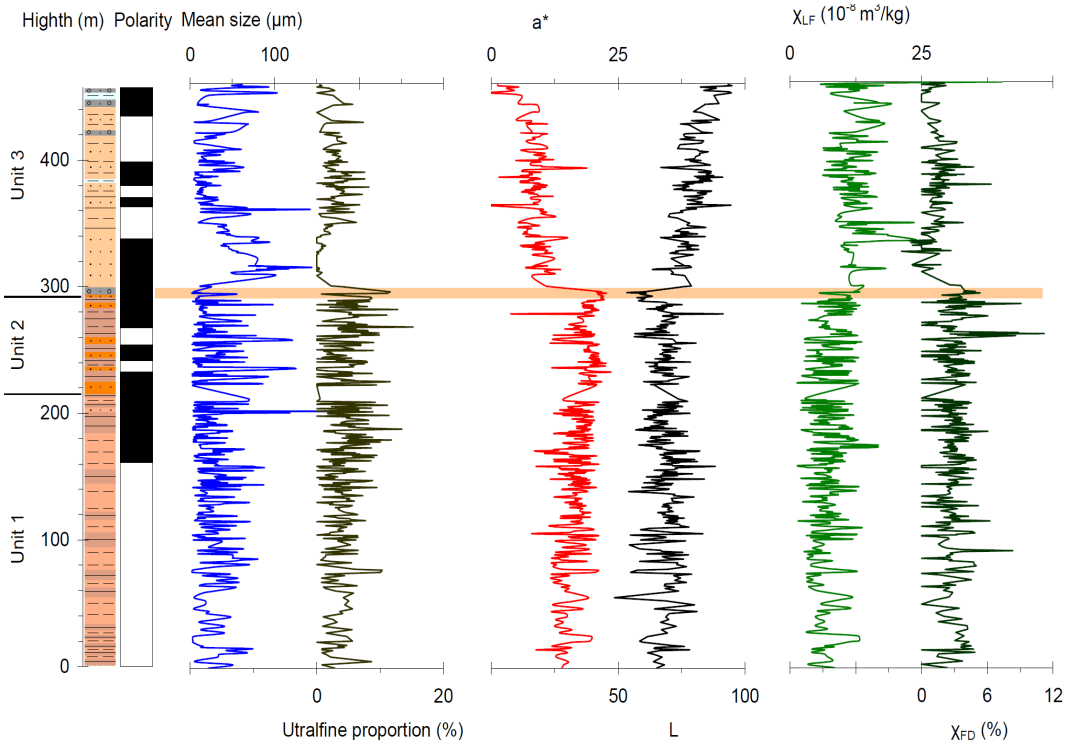

Fig. 3. Multi-proxy records of the HBS Section. The lithology types of the strata are the same as in Fig. 1.

CPD
9, 2661–2680, 2013

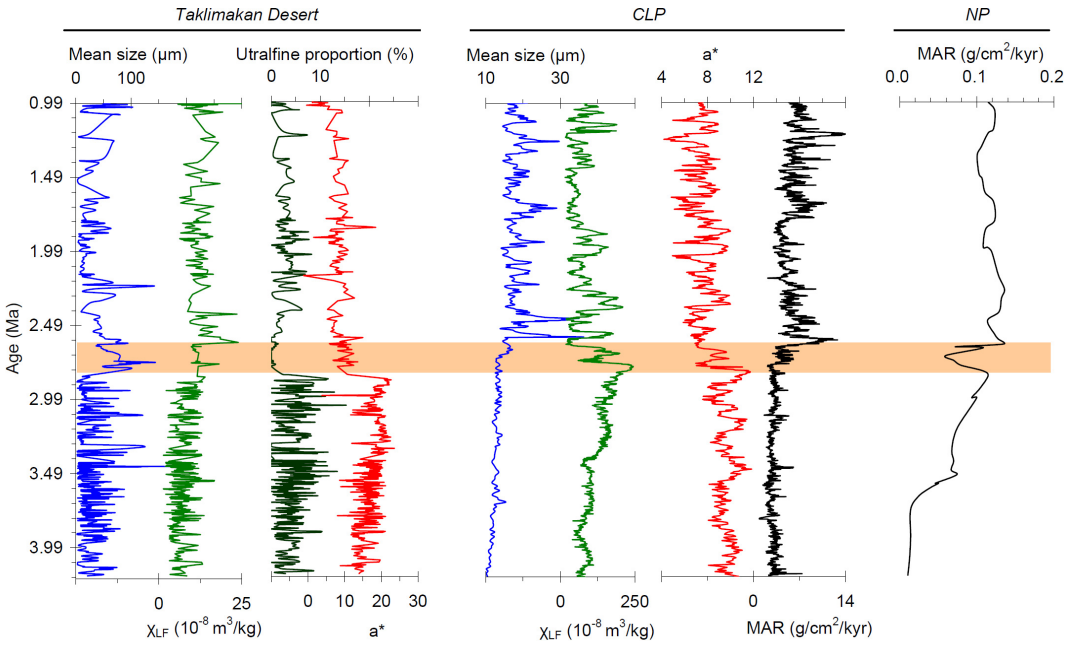

Fig. 4. Time series of the multi-proxy indices from the HBS Section and their correlation with those from CLP (Sun et al., 2008, 2010; Wang et al., 2012b; Sun and An, 2005) and NP (Rea et al., 1998).

CPD
9, 2661–2680, 2013